NOTE • OPEN ACCESS

A direct-writing electrospinning system for designing complex architectures in tissue engineering

Biomedical Physics & Engineering Express

NOTE

A direct-writing electrospinning system for designing complex architectures in tissue engineering

Laura Armenio[1], Silvia Farè[1,2] and Lorenza Draghi[1,2]

[1] Department of Chemistry, Materials and Chemical Engineering 'G. Natta', Politecnico di Milano, via Mancinelli 7, 20131 Milan, Italy
[2] INSTM, National Interuniversity Consortium of Materials Science and Technology, Local Unit Politecnico di Milano, Piazza Leonardo da Vinci 32, 20133 Milan, Italy

E-mail: laura.armenio@polimi.it

Keywords: direct-writing electrospinning, tissue engineering, nature-derived polymers

Supplementary material for this article is available online

OPEN ACCESS

RECEIVED
25 August 2023

REVISED
28 November 2023

ACCEPTED FOR PUBLICATION
16 January 2024

PUBLISHED
24 January 2024

Abstract

Recently, direct-writing electrospinning has been pursued to reach a higher accuracy and complexity in fiber scaffold fabrication compared to other extrusion techniques more frequently encountered in tissue engineering. However, to date, direct-writing electrospinning lacks a wide application to process materials such as nature-derived polymers, of huge importance in tissue engineering given their chemical properties similar to that of native tissues. In this work, a setup to perform direct-writing electrospinning was developed and demonstrated versatility and efficiency in obtaining submicrometric fibers and guiding their deposition along various types of paths and patterns, resulting in a user-friendly method to create structures closely resembling tissue architecture.

1. Introduction

By applying an electric field between a spinneret and a moving platform, direct-writing electrospinning (DWE) combines the typical control over material deposition of additive manufacturing (AM) with the capability of electrospinning (ES) to lay down submicrometric filaments. In this way, DWE enables to control fiber deposition and fabricate complex fibrous structures which are challenging to obtain with ES and replicate more realistically the fibrous architecture of biological tissues with respect to AM.

Moreover, if compared to cell-electrospinning, DWE does not imply cells embedding directly inside the ink which, under the application of a voltage difference and in direct contact with the solvents usually employed for electrospinning [1], can undergo necrosis, but it is able to reach a high structures resolution without impairing cell survival.

To control fiber deposition in DWE, maintaining the electrospun jet in its straight region is essential and this can be obtained by near-field electrospinning (NFES) or melt electrowriting (MEW). The absence of a whipping phase results in generally larger diameter compared to traditional electrospinning, but significantly smaller if compared to other widely used extrusion techniques (the minimum obtainable filament diameter being roughly less than 0.1 μm [2] in NFES or 5 μm [3] in MEW versus 100–200 μm [4–7]), reaching a higher resolution.

DWE potential to guide cell orientation and maturation has been widely confirmed by processing synthetic polymers, especially poly(ε-caprolactone) (PCL). Using MEW, diagonal PCL fibers led to a pronounced fibroblasts elongation and scaffold morphological features made cells interact as a 3D construct rather than a flat substrate [8] whereas seeded on hexagonal PCL scaffolds had a positive influence on human induced pluripotent stem cell-derived cardiomyocytes in terms of beating rate, cell alignment, sarcomere content and organization as compared to rudimentary fiber scaffolds [9].

Adopting NFES, poly-L-lactic acid (PLLA) quadrangular or rhomboidal (0°/45°) grids were also collected under optimized process conditions [10], which made human umbilical artery smooth muscle cells largely aligned and elongated and cell infiltration 4.5-fold greater than control electrospun scaffolds, whereas triangular or diamond-shaped porous scaffolds made by PCL and hydroxyapatite [11] showed excellent connectivity with no closed pores and mouse pre-osteoblasts could spread, proliferate and differentiate for an extended time, *in vitro*.

Table 1. Range of parameters varied for DWE optimization and system validation with PEO solution.

XY velocity [mm/min]	Needle-collector distance [mm]	Electric field [kV/mm]	Flow rate [μl/h]
2000, 4000, 8000	1, 3, 10	1, 2	30

Table 2. Range of parameters varied for DWE optimization and system validation with GelB/BSA solution.

XY velocity [mm/min]	Needle-collector distance [mm]	Electric field [kV/mm]	Flow rate [μl/h]
8000	2, 3	1, 1.5	22

Despite its potential, to date DWE applicability is still very limited, especially in dealing with nature-derived polymers, which are typically more challenging to be processed via electric-field based techniques [12], even though they possess extracellular matrix-like features, mechanical tunability, high biocompatibility, and high water holding capacity, all appealing for tissue regeneration [13]. Some applications of DWE to process natural polymers have been reported in [14], where gelatin fibers were parallelly placed onto silicon or polydimethylsiloxane (PDMS) substrates and a significant endothelial cell line attachment was observed, not present on featureless 2D surfaces. Fibrous alginate patterned in parallel lines [15] demonstrated how interfiber spacing influenced cell alignment and viability, defining an optimal range to guide cellular orientation and maintain an adequate viability not only with clusters but even at single cell level. The remaining studies involving DWE and nature-derived polymers report blends of the latter with synthetic polymers: PCL and collagen grids obtained via NFES [16] not only guided human periodontal ligament stem cells disposition, but also promoted their differentiation in periodontal ligament cells with respect to randomly electrospun fibers. NFES was also used to fabricate scaffolds made by a blend of PCL and an anti-inflammatory drug (F101) [17] which after being implanted in a mouse supported an improved wound recovery.

Here, a simple but highly controllable and user-friendly DWE setup was developed. Components were assembled in a configuration that ensures easy replicability, transferability of the system and fast set-up of the DWE procedure, to provide an alternative easily adaptable to experimental conditions. The capabilities of control and actuation system to accurately reproduce a desired motion trajectory and exert a control over fiber placement were here assessed with a synthetic polymer (polyethylene oxide, PEO) and then the possibility of processing more complex materials such as natural polymers was validated, using a blend of Gelatin B and Bovine Serum Albumin, never tested before with DWE: the solution was chosen as a model for large availability and favourable properties of both polymers, such as the similarity of Gelatin B to collagen, the most naturally found protein in humans and animals [18] and the non-oxidant properties of Bovine serum Albumin [19] that tend to reduce cell damaging.

Structures obtained with the system were also biologically tested, proving DWE setup efficiency in depositing highly organized and controlled fiber patterns able to guide cellular orientation and disposition.

2. Materials and methods

2.1. Setup assembly

The setup XY motion was obtained equipping the XY motion platform (ACRO System, OpenBuilds, $40 \times 28 \times 15$ cm^3) with an actuation provided by 3 GT2 belts (belt width = 5 mm), 3 GT2 pulleys (36 teeth, $\varnothing_{bore}$ = 5 mm, $\varnothing_{pulley}$ = 2.29 cm) and 12 wheels ($\varnothing_{wheel}$ = 2.4 cm) and driven by 3 NEMA 17 stepper motors ($\varnothing_{shaft}$ = 5 mm, V_{in} = 12 V). In particular, pulleys and wheels diameters were selected to have a reduction ratio ($\varnothing_{wheel}/\varnothing_{pulley}$) as close as possible to 1, to avoid slipping between wheels and belt.

A 3D printed polylactic acid (PLA) plate was screwed on the XY translating element of the platform (figure 1) and an aluminum plate ($12 \times 12 \times 0.5$ cm^3) was assembled on the PLA one with nuts and screws to allow the levelling of the fiber collecting surface.

The control system was made by Arduino Uno (V_{in} = 5–12 V) and CNC Shield v3.0 (V_{in} = 12–36 V) boards with 4 A4988 drivers (V_{in} = 8V–35V) assembled, connected to the PC through a USB 2.0 cable Type A/B and fed by a voltage supply (12 V, 20 A). The reduction of the control system was set as 1/16, so that each motor step is converted into a movement of the driven wheel equal to 1/16 of the pulley rotation, the smallest motion entity possible with NEMA 17 motors.

LaserGRBL software was used to send motion trajectories to the XY motion platform and to set other key motion parameters. The wide variety of file extensions (.SVG, .JPEG, .PNG or .STL file) accepted and authomatically converted into .GCODE results in an easy-to-use and versatile PC interface. Acceleration was set as 1500 mm/s^2 to ensure a fast reaching of the set velocity value, while step/mm value was equal to 53.33 for X and Y motion axes to make the XY moving platform accomplish motion translations coherent with the trajectory extension.

On the top of the XY moving plate, a syringe pump (NewEra Pump Systems) was positioned to dispense the polymeric solution for DWE and electrostatic generators (Enrico Pesatori Costruzioni Elettriche, V_{max} = 20 kV) were used to initiate the DWE procedure between the spinneret and the XY moving plate.

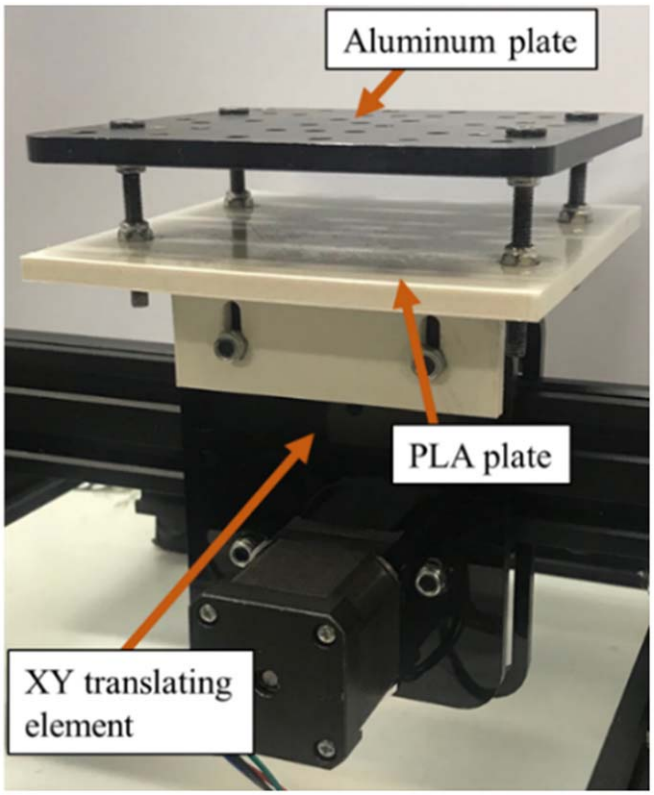

Figure 1. XY translating plate of the DWE system: the aluminum collector plate, the white 3D printed PLA plate fixed to the XY translating element and the 4 screws with nuts for fine leveling of the collecting plane.

2.2. XY motion system characterization

To control the correct command transfer from PC to XY platform, speed values were increasingly set on LaserGRBL and the consequent control system output signal frequency was measured by detecting the signal with an oscilloscope (XDS3104E, Owon), verifying proportionality between speed and frequency increments. The actual XY moving plate velocity was recorded by measuring the time necessary for the plate to complete the trajectory while performing specific squared trajectories (3 measurements per velocity value).

2.3. Parameters optimization and system validation

A 20% w/v PEO (Sigma Aldrich, average Mv = 200000, powder, CAS Number: 25322-68-3, PCode: 1002328129) solution in a 6:4 mixture of deionized water and ethanol was chosen for experimental testing. A 20 G non-beveled needle was used as a spinneret. The needle was positively charged, while the XY moving plate was negatively charged. Fibers were collected on a stainless steel plate covered with aluminum foil, placed on top of the XY moving plate. Process parameters (XY collector velocity, needle-collector distance, electric field and solution flow rate) were varied according to the range reported in table 1 to investigate their effect on different motion trajectories.

2.4. Fabrication of protein-based scaffold

After system optimization and validation, the DWE system potential of processing even nature-derived polymers in addition to synthetic polymers was also evaluated. In particular, two natural polymers not yet investigated via DWE, Gelatin from bovine skin (GelB, Sigma Aldrich, powder, CAS number: 9000-70-8, PCode: 1002978963) and Bovine Serum Albumin (BSA, Sigma Aldrich, lyophilized powder, CAS number: 9048-46-8, PCode: 1002494455) were blended 10:1 in 70% v/v aqueous acetic acid (total concentration 22, 27.5, 44% w/v) and both solution and DWE process (electric field, flow rate, needle gauge and XY speed) were optimized (range of parameters reported in table 2) to deposit straight submicrometric fibers in parallel arrays (20×20 mm^2) at different interfiber spacings (0, 500 and 1000 μm) and in circles (Ø = 26 mm), to demonstrate whether the DWE system was able to guide submicrometric fibers along straight and curved trajectories.

To address biological characterization, multi-layered oriented fibrous samples were obtained by depositing methacrylated gelatin and BSA 22% w/v in 70% v/v aqueous acetic acid in parallel arrays of fibers on a soft hydrogel (h_{wet} = 500 μm, Ø = 6 mm) made by the same natural polymers dissolved in DPBS (EuroClone, PCode: ECB4053) to allow an easy handling of patterns and preventing their damage during *in vitro* cellular tests (figure 2). Both fiber spacing and

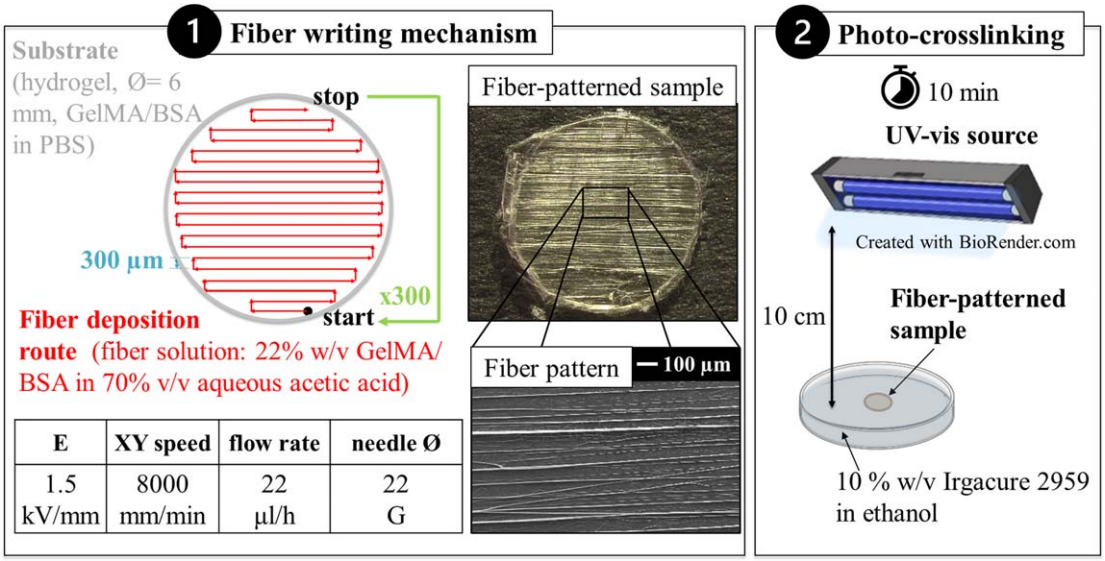

E	XY speed	flow rate	needle Ø
1.5 kV/mm	8000 mm/min	22 µl/h	22 G

Figure 2. Scheme of DWE fiber-writing strategy and subsequent photo-crosslinking to obtain multilayered oriented samples.

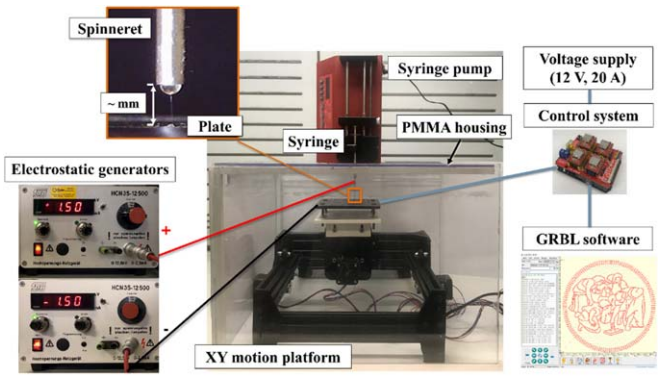

Figure 3. Scheme of the DWE setup.

amount of deposition cycles were optimized and set as 300 μm and 300 respectively towards fibers with suitable diameters and straightness to address anisotropic tissues engineering. GelB was substituted by GelMA to make structures not soluble in aqueous environment: in particular, the so-obtained structures were crosslinked by immersing them in Irgacure 2959 (Fluorochem, CAS number: 106797-53-9, PCode: F234409) 10% w/v in ethanol for 2 h and exposed at UV light at 10 cm for 10 min, still being immersed in photocuring agent solution. This procedure made structures resistant against PBS immersion for up to 23 d at 37 °C.

2.5. Biological evaluation

Multilayered samples were then UV sterilized, immersed in DPBS and DMEM (EuroClone, PCode; ECB7501L) for 5 min and 4 h respectively, to avoid the risk of a possible acetic acid residual release in culture. C2C12 murine cells were seeded on them (density = 20000 cells/cm^2), and at 1, 3 and 7 d of culture

Table 3. XY velocity values set on LaserGRBL and the corresponding effective XY velocities of the XY motion platform.

Set XY velocity [mm/min]	Effective XY velocity [mm/min]		Relative error [%]
	Mean	SD	
500	495	4	1
1000	970	6	3
2000	1891	7	5
4000	3709	55	7
8000	6733	63	16

AlamarBlue resazurin assay (Resazurin sodium salt, BioReagent, suitable for cell culture, Sigma Aldrich, PCode: R7017) was performed to evaluate cell growth, by dividing the fluorescence (RFU) signal detected by a spectrophotometer at each time point to that recorded at culture day 1, at the excitation and emission wavelength of 554 and 593 nm respectively, according to the below equation (equation (1)):

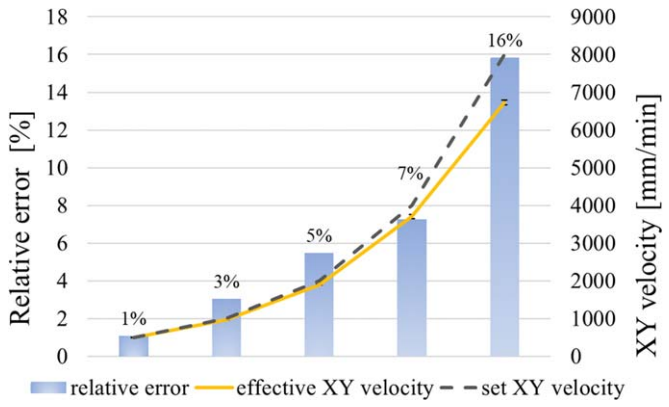

Figure 4. Comparison between set XY velocity (dashed line) and effective XY velocity (yellow-coloured line) of the XY motion platform, with the relative error between them (blue-coloured histogram).

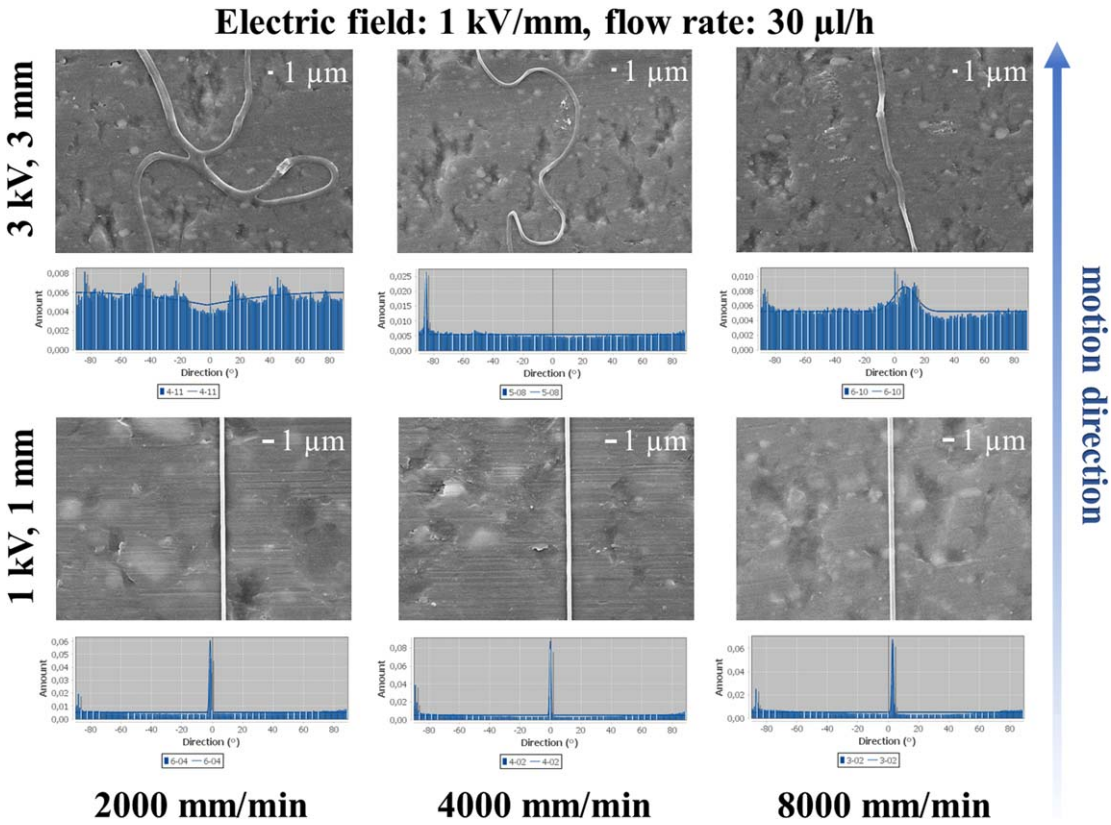

Figure 5. SEM images of single PEO fibers collected, with the corresponding directionality hystograms (electric field: 1 kV/mm, flow rate: 30 μl/h, n° of motion trajectory executions: 1). The presence of a sharp peak indicates high fiber orientation.

$$\text{Cell growth}[\%] = \text{RFUt}/\text{RFU1d} \quad (1)$$

After 8 days in culture, cells were fixed and stained with Rhodamine Phalloidin (ThermoFisher, Mol. Prob. R415) to stain F-actin, Hoechst 33342 (ThermoFisher, Mol. Prob. H1399) to observe nuclei. Cells orientation and adhesion on the samples were visualized by fluorescence microscopy (BX51WI, Olympus).

2.6. Morphological characterization

Fiber diameter and alignment along the motion direction were evaluated by Stereo Microscopy (S9i, Leica) and Scanning Electron Microscopy (SEM, EVO 50, Zeiss) and image analysis was performed through ImageJ [20]: for each filament, the diameter was measured in three points along the entire filament length and directionality hystograms were generated through the Directionality tool to evaluate fiber straightness and alignment along the motion trajectory.

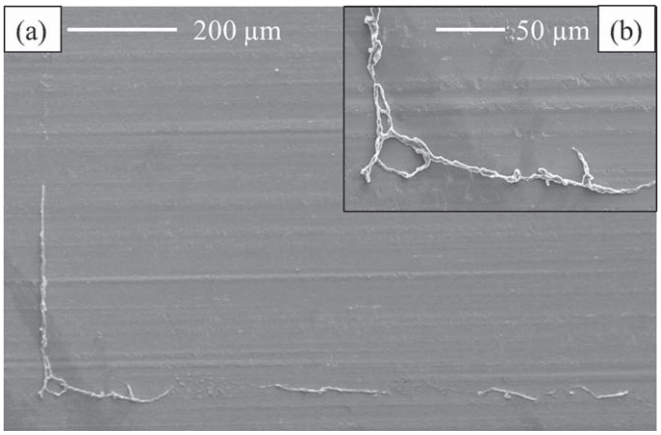

Figure 6. SEM images of corners of the square route performed by the XY motion platform, with 100× (a) and 500× (b) magnification (electric field: 1 kV/mm, needle-collector distance: 3 mm, flow rate: 30 µl/h, n° of motion trajectory executions: 1).

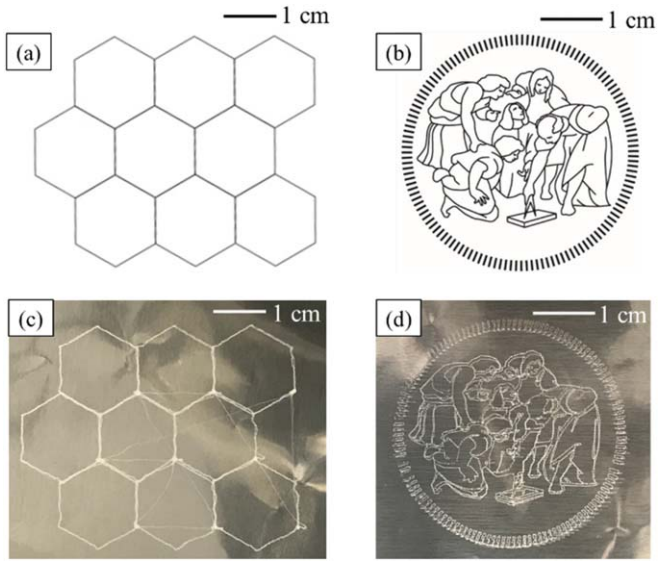

Figure 7. JPEG file loaded into LaserGRBL software depicting a honeycomb (a), the Politecnico di Milano logo (b) and the corresponding fiber patterns obtained (c), (d) (electric field: 2 kV/mm, needle-collector distance: 10 mm, flow-rate: 30 µl/h, n° of motion trajectory executions: 99).

Cells nuclei were quantified via the Analyze Particles tool, selecting only particles with area greater than 30 μm^2 to exclude particles different from cells and after a proper thresholding and watershed binary analysis.

2.7. Statistical analysis

Data were expressed as mean ± standard deviation. Statistical analyses were performed with GraphPad Prism 8. A value of $p < 0.05$ was considered statistically significant.

3. Results

The developed setup is reported in figure 3. The control system evaluation through oscilloscope highlighted a signal frequency increase directly proportional to velocity values set at the PC interface up to 9000 mm/min: at higher speed values, the proportionality with the set speed was not maintained. Thus, 9000 mm/min can be regarded as the maximum speed value applicable to the XY motion platform.

Considering the XY plate movement, the error between the effective and the set XY velocity increased with velocity values, remaining down to 7% for speed below 4000 mm/min; at 8000 mm/min, the highest error (16%) was found (figure 4).

In table 3, the effective XY velocities of the motion platform corresponding to the values set on LaserGRBL software with the relative error between the two velocities are reported.

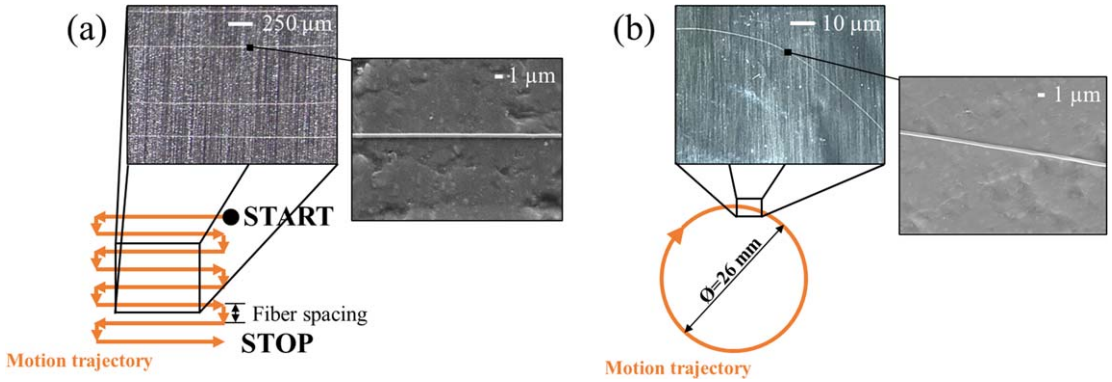

Figure 8. Motion trajectory schemes and photos of fiber composing patterns (a): parallel array (b): circle (taken at stereoptical microscope and at SEM).

Table 4. Values of mean fiber diameter and standard deviation for both parallel arrays and circles (n = 61, n = 6 respectively), obtained at 1.5 kV/mm, 8000 mm/min, 22 µl/h, 22 G.

	Mean fiber Ø [µm]	SD [µm]
Parallel arrays	0.72	0.21
Circles	1.04	0.27

After DWE system development and XY motion platform characterization, setup capability of fiber guidance was assessed. In tests conducted with PEO solution varying needle-collector distances and XY motion velocities while maintaining a constant electric field (1 kV/mm) and performing a 40-mm squared motion trajectory, it was observed that by reducing the travel distance and increasing XY collector velocity, fiber straightness and alignment were improved.

At 1 mm, straight submicrometric fibers were reached at each velocity value tested, as demonstrated by the sharp peaks present in directionality hystograms (figure 5).

At trajectory corners, shape accuracy was maintained but fiber straightness is impaired, due to the XY motion platform deceleration when it approaches the direction inversion point (figures 6(a), (b)), with the collection of coiled and discontinuous fiber. However, from literature [21], it is recommended the use of patterns near the high-speed region only, discarding the fiber portions near acceleration and deceleration regions.

The system was able to lay down fibers according even to intricated motion trajectories (figures 7(c), (d)), maintaining a dimensional correspondance with the original trajectory image (figures 7(a), (b)) at a needle-collector distance of 10 mm applying 2 kV/mm as electric field, even if fibers lost their straightness appearing coiled and wavy. Nevertheless, an important advantage of the DWE setup consists in the versatility ensured in terms of motion trajectory file format, which does not need to be converted in GCode file with auxiliary programmes as in other techniques to be read properly by the XY platform (e.g. slicing software for 3D printing) but can be authomatically translated in form of GCode commands by the PC interface itself. This overcomes a great limitation of current DWE systems: the lack of easy programming strategies and of predefined command libraries for the XY plate motion, which makes it hard to reach complex scaffold geometries with DWE [22]. Indeed, literature shows plenty of grid-like scaffolds built via DWE [23–28] and only few exceptions show a higher degree of pattern intricacy [11, 29–33].

Moreover, the vast majority of DWE systems are built 'in-house' with broad differences in how each machine performs functions, which complicates the direct comparison of data and results among different research group and hampers the high-throughput production of structures, preventing the technique from becoming standard in scaffolds fabrication. Having a DWE setup which simplifies the motion commands transfer for the user can bring to increase consistently DWE usability and control.

For GelB/BSA solution, 22% w/v as total concentration allowed process stability and deposition of continuous fibers along different motion trajectories, even curved which have not yet been widely explored with DWE of nature-derived polymeric solutions and are difficult, if not impossible, to be obtained with conventional electrospinning. As electric field, 1 kV/mm gave rise to a not continuous fiber writing and to fiber diameters not uniform and micrometric (1.37 ± 0.97 μm). Straight fibers were obtained at 1.5 kV/mm, 8000 mm/min, 22 μl/h, 22 G for both parallel fibers and circles (figures 8(a), (b)), apart from some confined coiled regions in correspondence with deceleration of the XY motion platform; in linear trajectories, fiber diameters were submicrometric, while for circular paths the mean fiber diameter resulted in falling into the micrometric range. Mean fiber diameters (mean fiber Ø) and standard deviation (SD) for both trajectories are reported in table 4.

After having validated the system ability to precisely lay down natural polymers according to a

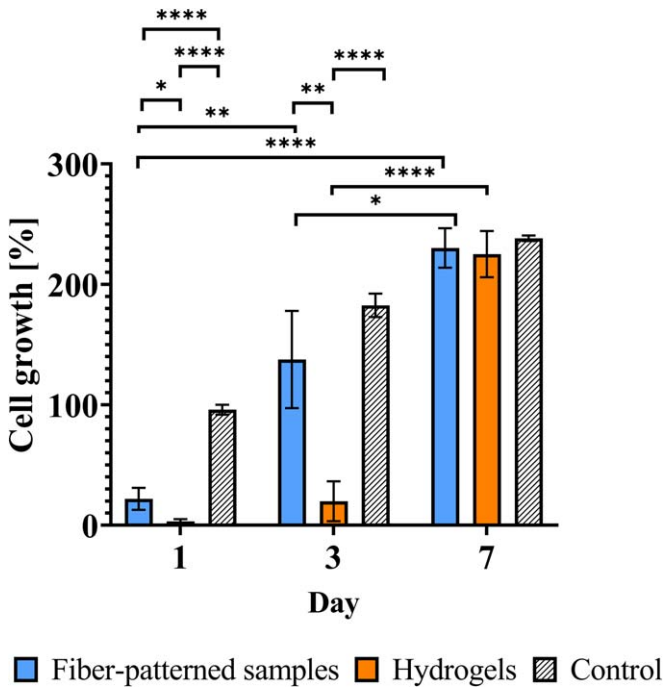

Figure 9. Cell growth on fiber-patterned samples, plain hydrogels and controls.

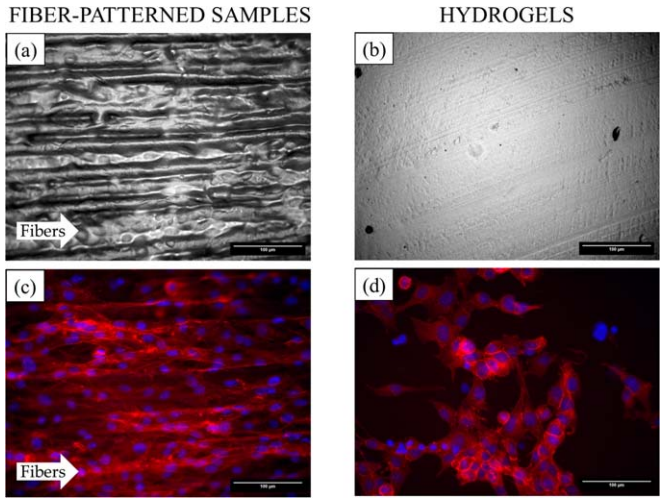

Figure 10. Images of fiber-patterned samples and plain hydrogels taken at 8 culture d: (a), (b) bright-field and (c), (d) IF images (red: phalloidin, blue: Hoechst). The white arrow represents fiber direction. Scale bar is 100 μm.

fibrous pattern of interest, multilayered oriented structures mimicking anisotropic tissues architecture (e.g. skeletal muscle tissue) were fabricated through DWE with a high degree of fiber alignment (70%) and in an automated and reproducible way.

In particular, a 300 μm interfiber spacing was selected as the best to ensure both fiber straightness and fiber diameters thinner. 300 repetitions of motion trajectory were estimated as the maximum to keep fiber alignment over the whole process.

From tests with C2C12 cell line, fiber-patterned structures demonstrated a progressive cell growth on them highlighted by the resazurin assay (figure 9), reaching after 7 d a comparable value with respect to the positive control (multiwell bottom) and to the hydrogels without fibers on top.

By Hoechst/Phalloidin staining at 8 d (figure 10), fiber-patterned samples were observed in their ability to guide cell orientation along with the fiber pattern direction. In fact, on average, 3-fold cells (1239 cells/mm^2 versus 430 cells/mm^2) were adhered on fiber-patterned samples with respect to plain hydrogels and moreover cells were spread and well elongated along fiber pattern direction, which confirms that the DWE system can create fiber patterns suitable for cell guidance.

4. Conclusion

The DWE system developed was found to be simple and cost-effective, and allows efficient control over process parameters for material lay-down. Submicrometric and very straight fibers can be deposited according to various shapes, even complex architectures, with only minor coiling when motion direction abruptly changes sometimes occurring. The DWE setup proved its capability to prepare patterns capable of exerting cell guidance.

On the whole, the DWE system presented can contribute to extend the use of this technique in the field of regenerative medicine and tissue engineering.

Data availability statement

All data that support the findings of this study are included within the article (and any supplementary files).

ORCID iDs

Laura Armenio https://orcid.org/0009-0002-8579-3419
Silvia Farè https://orcid.org/0000-0002-0303-1131
Lorenza Draghi https://orcid.org/0000-0003-4744-7777

References

[1] Maurmann N, França F S, Girón J and Pranke P 2023 Cell electrospinning: a review of materials and methodologies for biofabrication *Adv. Biology* **7** 2300058
[2] Park Y S, Kim J, Oh J M, Park S, Cho S, Ko H and Cho Y K 2020 Near-field electrospinning for three-dimensional stacked nanoarchitectures with high aspect ratios *Nano Lett.* **20** 441–8
[3] Loewner S, Heene S, Baroth T, Heymann H, Cholewa F, Blume H and Blume C 2022 Recent advances in melt electro writing for tissue engineering for 3D printing of microporous scaffolds for tissue engineering *Front. Bioeng. Biotechnol.* **10** 896719
[4] Germain L, Fuentes C A, van Vuure A W, des Rieux A and Dupont-Gillain C 2018 3D-printed biodegradable gyroid scaffolds for tissue engineering applications *Mater. Des.* **151** 113–22
[5] Molde J, Steele J A M, Pastino A K, Mahat A, Murthy N S and Kohn J 2020 A step toward engineering thick tissues: distributing microfibers within 3D printed frames *J. Biomed. Mater. Res.* A **108** 581–91
[6] Oh C H, Hong S J, Jeong I, Yu H S, Jegal S H and Kim H W 2010 Development of robotic dispensed bioactive scaffolds and human adipose–derived stem cell culturing for bone tissue engineering *Tissue Eng.* C **16** 561–71
[7] Moroni L *et al* 2018 Biofabrication: a guide to technology and terminology *Trends Biotechnol.* **36** 384–402
[8] Farrugia B L, Brown T D, Upton Z, Hutmacher D W, Dalton P D and Dargaville T R 2013 Dermal fibroblast infiltration of poly(ε-caprolactone) scaffolds fabricated by melt electrospinning in a direct writing mode *Biofabrication* **5** 0250016
[9] Castilho M, van Mil A, Maher M, Metz C H G, Hochleitner G, Groll J, Doevendans P A, Ito K, Sluijter J P G and Malda J 2018 Melt electrowriting allows tailored microstructural and mechanical design of scaffolds to advance functional human myocardial tissue formation *Adv. Funct. Mater.* **28** 1803151
[10] Yuan H, Zhou Q, Li B, Bao M, Lou X and Zhang Y 2015 Direct printing of patterned three-dimensional ultrafine fibrous scaffolds by stable jet electrospinning for cellular ingrowth *Biofabrication* **7** 045004
[11] He F L, Li D W, He J, Liu Y Y, Ahmad F, Liu Y L, Deng X, Ye Y J and Yin D C 2018 A novel layer-structured scaffold with large pore sizes suitable for 3D cell culture prepared by near-field electrospinning *Mater. Sci. Eng.*C **86** 18–27
[12] Wang Y, Aslam Khan M, Chen K, Zhang L and Chen X 2023 Electrospinning of natural biopolymers for innovative food applications: a review *Food. Bioprocess. Tech.* **16** 704–25
[13] ter Horst B, Moiemen N S and Grover L M 2019 Natural polymers: biomaterials for skin scaffolds *Biomaterials for Skin Repair and Regeneration* ed E Garcìa-Gareta (Elsevier: Woodhead Publishing) 6 151–92
[14] Xue N, Li X, Bertulli C, Li Z, Patharagulpong A, Sadok A and Huang Y Y S 2014 Rapid patterning of 1-D collagenous topography as an ECM protein fibril platform for image cytometry *PLoS One* **9** e93590
[15] Fuh Y K, Wu Y C, He Z Y, Huang Z M and Hu W W 2016 The control of cell orientation using biodegradable alginate fibers fabricated by near-field electrospinning *Mater. Sci. Eng.* C **62** 879–87
[16] Ren S, Yao Y, Zhang H, Fan R, Yu Y, Yang J, Zhang R, Liu C, Sun W and Miao L 2017 Aligned fibers fabricated by near-field electrospinning influence the orientation and differentiation of hPDLSCs for periodontal regeneration *J. Biomed. Nanotechnol.* **13** 1725–34
[17] Tsai L C, Pan C T, Yen C K, Wang S Y, Yang A Y, Kuo S W, Wu S Y and Wen Z H 2017 Study of the drug fiber for wound healing by direct-writing near field electrospinning with subdivision control *International Conference on Applied System Innovation (ICASI), Sapporo* 13-17, 412–5
[18] Alipal J, Mohd Pu'ad N A S, Lee T C, Nayan N H M, Sahari N, Basri H, Idris M I and Abdullah H Z 2021 A review of gelatin: Properties, sources, process, applications, and commercialisation *Mater. Today Proc.* **41** 240–50
[19] Mishra V and Heath R J 2021 Structural and biochemical features of human serum albumin essential for eukaryotic cell culture *J. Mol. Sci.* **22** 8411
[20] Schindelin J *et al* 2012 Fiji: an open-source platform for biological-image analysis *Nat. Methods* **9** 676–82
[21] Phung T H, Oh S and Kwon K S 2018 High-resolution patterning using two modes of electrohydrodynamic jet: drop on demand and near-field electrospinning *J. Vis. Exp.* **137** e57846
[22] King W E III and Bowlin G L 2021 Near-field electrospinning and melt electrowriting of biomedical polymers—progress and limitations *Polymers* **13** 1097
[23] Yan F, Chen H, Zheng L, Chen W, Liu Y and Hu Q 2013 The controllable PVA-chitosan fiber prepared by the near-field electro spinning for tissue engineering *Adv. J. Food Sci. Technol.* **5** 1073–8
[24] Brennan C M, Eichholz K F and Hoey D A 2019 The effect of pore size within fibrous scaffolds fabricated using melt electrowriting on human bone marrow stem cell osteogenesis *Biomed. Mater.* **14** 065016
[25] Hochleitner G, Hümmer J F, Luxenhofer R and Groll J 2014 High definition fibrous poly(2-ethyl-2-oxazoline) scaffolds through melt electrospinning writing *Polymer* **55** 5017–23
[26] Hochleitner G, Kessler M, Schmitz M, Boccaccini A R, Teßmar J and Groll J 2017 Melt electrospinning writing of defined scaffolds using polylactide-poly(ethylene glycol) blends with 45S5 bioactive glass particles *Mater. Letter.* **205** 257–60
[27] Yoshida M, Turner P R, Azam Ali M and Cabral J D 2021 Three-dimensional melt-electrowritten polycaprolactone/chitosan scaffolds enhance mesenchymal stem cell behavior *ACS Appl. Bio Mater.* **4** 1319–29
[28] Davis Z G, Hussain A F and Fisher M B 2021 Processing variables of direct-write, near-field electrospinning impact size and morphology of gelatin fibers *Biomed. Mater.* **16** 045017

[29] Zheng G, Jiang J, Wang X, Li W, Yu Z and Lin L 2021 High-aspect-ratio three-dimensional electrospinning via a tip guiding electrode *Mater. Des.* **198** 109304
[30] Olvera D, Molina M S, Hendy G and Monaghan M G 2020 Electroconductive melt electrowritten patches matching the mechanical anisotropy of human myocardium *Adv. Funct. Mater.* **30** 1909880
[31] Bakirci E, Schaefer N, Dahri O, Hrynevich A, Strissel P, Strick R, Dalton P D and Villmann C 2020 Melt electrowritten in vitro radial device to study cell growth and migration *Adv. Biosyst.* **4** 2000077
[32] Paxton N C *et al* 2020 Design tools for patient specific and highly controlled melt electrowritten scaffolds *J. Mech. Behav.* **105** 103695
[33] Liashenko I, Hrynevich A and Dalton P D 2020 Designing outside the box: unlocking the geometric freedom of melt electrowriting using microscale layer shifting *Adv. Mater.* **32** 2001874